CIAO1 as a crucial signature gene of cuproptosis in gastric cancer

JIAYING QU[1*], CHUNHUI YANG[2*], SHUNCHEN ZHOU[1], BOSEN ZHAO[1], QIANGSONG TONG[2] and LIDUAN ZHENG[1]

[1]Department of Pathology, Union Hospital, Tongji Medical College, Huazhong University of Science and Technology, Wuhan, Hubei 430022, P.R. China; [2]Department of Pediatric Surgery, Union Hospital, Tongji Medical College, Huazhong University of Science and Technology, Wuhan, Hubei 430022, P.R. China

Received December 12, 2024; Accepted May 13, 2025

DOI: 10.3892/ol.2025.15186

Abstract. Gastric cancer is a global health challenge, necessitating the identification of novel biomarkers and therapeutic targets. The present study aimed to assess the role of cuproptosisrelated genes (CRGs) in gastric cancer, with the goal of establishing a predictive model consisting of key regulators with prognostic significance, thereby enabling the identification of key genes. Data from The Cancer Genome Atlas and Gene Expression Omnibus databases were used to analyze CRGs in stomach adenocarcinoma (STAD). Least absolute shrinkage and selection operator regression analysis was applied to create a risk model, and its predictive accuracy was confirmed for several clinical subgroups. Moreover, the prognostic value of essential regulators was evaluated through multiple analyses. A risk model with 15 CRGs was used to effectively predict STAD prognosis, demonstrating areas under the receiver operating characteristic curve values of 0.822, 0.811 and 0.922 for 1-, 3- and 5-year overall survival rates, respectively. The risk scores were associated with survival and tumor site. Among the CRGs, the gene for cytosolic iron-sulfur assembly component 1 (*CIAO1*) was revealed to be critical and associated with histological type, age and treatment outcome. Moreover, single-cell analysis demonstrated that *CIAO1* is highly expressed in numerous types of cancer cells, and a high expression of *CIAO1* was associated with upregulated transcription levels of immune checkpoints, increased tumor mutation load and decreased immune scores, highlighting its complex role in the tumor microenvironment. *CIAO1* knockdown experiments were performed, and eliminating *CIAO1* was associated with a reduction in the levels of iron-sulfur proteins and an increase in heat shock protein 70 expression, thereby inducing copper-dependent cell death. Furthermore, treatment with the drugs dasatinib and AT-9283 were associated with an inhibition of *CIAO1* expression in gastric cancer cells, and decreased rates of tumor spread and invasion. Taken together, the findings of the present study suggest that *CIAO1* is a promising biomarker both for assessing prognosis and evaluating the tumor immune microenvironment of gastric cancer.

Introduction

Gastric cancer is one of the most common malignant tumors in the world, accounting for ~5% of all newly diagnosed cancer cases/year (1). However, due to a lack of distinct early symptoms and low regular screening rates, the majority of patients with gastric cancer are diagnosed at advanced stages, resulting in limited treatment efficacy and a poor prognosis (2,3). Consequently, there is an urgent need to identify novel biomarkers and therapeutic targets for the purposes of enhancing early diagnosis and treatment efficiency, and improving the survival rates of patients (4).

Copper, an essential trace element for human health, is involved in numerous signaling pathways, affecting the biological behavior of tumors. It is also a key component of certain enzymes that are essential for the mitochondrial respiratory chain and angiogenesis (5). Recent studies have reported that the intracellular accumulation of copper ions triggers both the aggregation of mitochondrial lipoacylated proteins and the destruction of iron-sulfur (Fe/S) cluster proteins, resulting in a unique form of cell death known as cuproptosis (6,7). The key genes associated with cuproptosis have been identified and are collectively referred to as cuproptosis-related genes (CRGs). These genes include, but are not limited to, the genes for ferredoxin 1 (*FDX1*), lipoic acid synthetase (*LIAS*), dihydrolipoamide dehydrogenase, pyruvate dehydrogenase E1 subunit α1 and PHD finger protein 2. These genes not only fulfill key

Correspondence to: Professor Liduan Zheng, Department of Pathology, Union Hospital, Tongji Medical College, Huazhong University of Science and Technology, 1277 Jiefang Avenue, Wuhan, Hubei 430022, P.R. China
E-mail: ld_zheng@mail.hust.edu.cn

*Contributed equally

Abbreviations: CRGs, cuproptosis-related genes; TCGA, The Cancer Genome Atlas; GEO, Gene Expression Omnibus; STAD, stomach adenocarcinoma; ROC, receiver operating characteristic; AUC, area under the ROC curve; DEGs, differentially expressed genes; GO, Gene Ontology; KEGG, Kyoto Encyclopedia of Genes and Genomes; TMB, tumor mutational burden; GSEA, gene set enrichment analysis

Key words: gastric cancer, cuproptosis, cytosolic ironsulfur assembly component 1, iron-sulfur cluster assembly, immunotherapy

roles in cuproptosis, but are also closely associated with tumor growth and clinical features (8). Chen *et al* (9) performed a comprehensive analysis of these genes in gastric cancer, and reported that expression levels of the CRGs were notably associated with clinicopathological features and the chemotherapy sensitivity of patients. In addition, through analyzing the cuproptosis-associated molecular subtypes of gastric cancer, Chong *et al* (10) reported that patients with specific subtypes exhibited a stronger response to immunotherapy and targeted therapy. However, the specific underlying regulatory mechanisms of cuproptosis and cuproptosis-associated signature genes in gastric cancer remain poorly understood, and further investigations of these genes and their signaling pathways are required to provide novel leads for the targeted therapy of gastric cancer.

Cuproptosis involves two main processes: Mitochondrial lipoylated protein aggregation and the depletion of Fe/S cluster proteins (10). The biosynthesis of Fe/S cluster proteins is coordinated by both intramitochondrial and extramitochondrial pathways, which, in turn, are mediated via the mitochondrial Fe/S cluster synthesis system or the cytoplasmic Fe/S cluster assembly (CIA), respectively. Cytosolic Fe/S assembly component (CIAO)1, a critical component of the CIA complex, performs an essential role in integrating Fe/S clusters into extramitochondrial Fe/S proteins. Within the CIA complex, CIAO1 specifically interacts with CIAO2A, CIAO2B and methyl methanesulfonate sensitivity gene 19 (MMS19) to form a functional unit (11,12). This CIAO1-CIAO2B-MMS19 complex binds to most cytoplasmic and nuclear Fe/S proteins, promoting their assembly (13,14). However, the exact mechanism through which CIAO1 affects cuproptosis and gastric cancer progression via regulating Fe/S cluster protein assembly has yet to be fully elucidated.

There is currently a pressing need to create a risk model and to identify biomarkers that are associated with cuproptosis, which are crucial for the early diagnosis and prognosis of gastric cancer. Therefore, the aim of the present study was to identify a cuproptosis-associated risk model and to investigate the specific functions of key genes.

Materials and methods

Data acquisition and processing. The expression matrix and clinical data of patients (TCGA-STAD) with gastric cancer were obtained The Cancer Genome Atlas (TCGA; https://portal.gdc.cancer.gov/) database. To enhance the reliability of the analysis, patients whose survival time was <30 days were excluded from the study. A final total of 348 clinical cases were randomly divided into two groups, each comprising 174 patients, with one used as a training set and the other as a testing set. A review of relevant literature was conducted using the PubMed database (https://pubmed.ncbi.nlm.nih.gov/) to identify genes associated with cuproptosis. The search strategy included the use of keywords such as 'cuproptosis', 'copper-induced cell death', and 'copper toxicity' in combination with terms like 'genes' and 'molecular mechanisms'. Articles published in peer-reviewed journals were considered during the search, and the inclusion criteria required studies to explicitly discuss the genetic or molecular mechanisms underlying cuproptosis. Exclusion criteria included review papers, studies focusing solely on non-genetic aspects, and those unrelated to copper-mediated cell death. The search covered the date range from March 2022 to May 2024. A total of 96 genes were identified from the selected studies. Using the R package 'limma' (version 3.58.1, bioconductor.org/packages/3.17/bioc/html/limma.html) for differential expression analysis, 41 CRGs were identified (15).

Single-cell sequencing data were acquired from the Gene Expression Omnibus (GEO; https://www.ncbi.nlm.nih.gov/geo/) database, specifically from dataset GSE163558. This dataset included three primary gastric cancer samples (GSM5004180, GSM5004181 and GSM5004182) and seven metastatic gastric cancer samples (GSM5004183, GSM5004184, GSM5004185, GSM5004186, GSM5004187, GSM5004188 and GSM5004189). These data were subsequently integrated and analyzed for further investigation.

The survival analysis data for CIAO1 were obtained from the Kaplan-Meier Plotter (http://kmplot.com/analysis/) to validate the impact of CIAO1 expression on the overall survival of patients with gastric cancer.

Establishment and verification of the risk model. After obtaining the 41 CRGs, 18 prognostic CRGs were subsequently identified using multivariate Cox analysis. Least absolute shrinkage and selection operator (LASSO) regression analysis was then performed, resulting in a risk model that included 15 of these prognostic CRGs. The expression levels of individual genes were multiplied by their specific coefficients to calculate a cumulative gene score for each patient, and the median cumulative gene score was used as a risk score to differentiate the patients into high- or low-risk groups. Receiver operating characteristic (ROC) curves were generated using the 'pROC' package (version 1.18.5, cran.r-project.org/package=pROC) (16) to predict survival rates at 1, 3 and 5 years. Additionally, nomograms were created using the 'survival' (version: 3.5.8, https://cran.r-project.org/package=survival) (17), 'regplot' (version: 1.1, https://cran.r-project.org/package=regplot) and 'rms' (version: 6.8.0, cran.r-project.org/package=rms) (18) packages to assess the accuracy and efficiency of the prediction model. These tools were essential for confirming the robustness of the model in terms of its predicting the survival outcomes of patients with gastric cancer.

Protein-protein interaction (PPI) network construction. To investigate the interactions between model genes, a PPI network was constructed using the STRING database (https://string-db.org). The analysis was performed with the interaction score set to a confidence threshold of 0.4 (medium confidence), and organism-specific settings were configured for Homo sapiens. Only experimentally validated interactions and those sourced from curated databases were included to ensure reliability.

Functional analysis of CIAO1. The CIAO1 expression data of TCGA-STAD samples were derived from the RNA-seq transcriptome dataset from TCGA). A t-test was used to assess the differences in expression between the tumor and normal samples. *CIAO1* expression was then compared across subgroups defined by several clinical characteristics,

including treatment outcome, histological type, tumor location, sex, pathological tumor (T)/lymph node (N) stage or age, using a Wilcoxon rank-sum test. Differentially expressed genes (DEGs) between these subgroups were identified using the R package 'limma' (version 3.58.1, bioconductor.org/packages/release/bioc/html/limma.html). To elucidate the biological processes and pathways associated with *CIAO1*, Gene Ontology (GO) and Kyoto Encyclopedia of Genes and Genomes (KEGG) enrichment analysis and Gene Set Enrichment Analysis (GSEA) were performed on the DEGs using the R packages 'clusterProfiler' (version 4.16.0, bioconductor.org/packages/release/bioc/html/clusterProfiler.html) and 'org.Hs.eg.db' (version 3.18.0, bioconductor.org/packages/release/bioc/html/org.Hs.eg.db.html) (19).

Tumor microenvironment analysis. The distribution of the *CIAO1* gene in patients with gastric cancer was assessed using the singlecell RNA-sequencing dataset, GSE163558. Dimensionality reduction was performed using t-distributed stochastic neighbor embedding. Principal cell types within this dataset were identified and annotated using the Leiden clustering method. The 'tidyverse' package (version 2.0.0, tidyverse.tidyverse.org/) was subsequently utilized to analyze the expression data of immune checkpoints in different *CIAO1* expression groups (20). Furthermore, the tumor mutational burden (TMB) was compared between these two groups using the 'maftools' package (version 2.18.0, bioconductor.org/packages/release/bioc/html/maftools.html) (21). Finally, the 'estimate' package (version 1.0.13, bioinformatics.mdanderson.org/estimate/) was utilized to calculate and compare immune scores between high- and low-*CIAO1* expression groups.

Evaluation of drug sensitivity. The CellMiner database (https://discover.nci.nih.gov/cellminer/home.do) was used to perform an analysis of drug sensitivity, integrating RNA expression data with drug activity information (22). The analysis was focused on drugs that had been approved through clinical trials by the United States Food and Drug Administration (FDA). Pearson correlation analysis was used to evaluate the correlation between *CIAO1* expression and drug sensitivity. Only results with significant significance ($P<0.05$) were retained. To ensure robust data processing and statistical evaluation, the 'impute' (version 1.76.0, bioconductor.org/packages/release/bioc/html/impute.html) and 'limma' (version 3.58.1, bioconductor.org/packages/release/bioc/html/limma.html) packages were utilized. Finally, the results were visualized using the 'ggplot2' (version 3.5.1, cran.r-project.org/package=ggplot2) and 'ggpubr' (version 0.6.0, cran.r-project.org/package=ggpubr) packages (23).

Cell culture. Human gastric mucosa GES-1 (cat. no. HTX1964; Otwo Biotech, Inc.) cells, gastric cancer AGS (cat. no. CL-0022; Pricella Biotechnology), SNU-1 (cat. no. CH1029; Newgainbio, Inc.), MKN-45 (cat. no. CL-0292; Wuhan Pricella Biotechnology Co., Ltd.), HGC-27 (cat. no. CL-0107; Wuhan Pricella Biotechnology Co., Ltd.) cells, 293 (cat. no. CL-0001; Wuhan Pricella Biotechnology Co., Ltd.) cells and cervical cancer HeLa (cat. no. CL-0101; Wuhan Pricella Biotechnology Co., Ltd.) cells were authenticated by short tandem repeat profiling, and used within 6 months after resuscitation of frozen aliquots. Mycoplasma contamination was regularly assessed using the LookOut® Mycoplasma PCR Detection Kit (cat. no. MP0035; Sigma-Aldrich; Merck KGaA). The gastric-related cell lines GES-1, SNU-1 and MKN-45 were cultured in RPMI-1640 (cat. no. PM150110; Wuhan Pricella Biotechnology Co., Ltd.) supplemented with 10% FBS (Gibco; Thermo Fisher Scientific, Inc.); the AGS cells were maintained in Ham's F-12K (cat. no. PM150910; Pricella Biotechnology) with 10% FBS; and HGC-27 was cultured in DMEM (cat. no. PM150210; Pricella Biotechnology Co., Ltd.) with 10% FBS. For non-gastric lines, 293 cells were maintained in DMEM (cat. no. PM150210; Pricella Biotechnology Co., Ltd.) with 10% FBS for adherent culture, and HeLa cells were cultured in MEM (cat. no. PM150411; Pricella Biotechnology Co., Ltd.) with 10% FBS. All cell lines were incubated under standard conditions at 37˚C with 5% CO_2.

Reverse transcription-quantitative PCR (RT-qPCR) analysis. Total RNA was extracted from human gastric cancer cell lines AGS and MKN-45 using the RNeasy® Mini kit (Qiagen GmbH) according to the manufacturer's instructions. Reverse transcription was carried out using the Transcriptor First Strand cDNA Synthesis Kit (Roche Diagnostics) with the following thermal protocol: 10 min at 65˚C for primer annealing, 30 min at 55˚C for reverse transcription, and 5 min at 85˚C for enzyme inactivation. qPCR was performed using PowerUp SYBR™ Green Master Mix (Thermo Fisher Scientific, Inc.) on the StepOne Real-Time PCR System (Thermo Fisher Scientific, Inc.). The thermocycling conditions were as follows: initial activation at 50˚C for 2 min and 95˚C for 2 min, followed by 40 cycles of denaturation at 95˚C for 15 sec and annealing/extension at 60˚C for 1 min. Quantification cycle (Cq) values were determined for each sample, and relative transcript levels were calculated using the $2^{-\Delta\Delta Cq}$ method, with β-actin serving as the internal reference gene (24). Primer sequences used in this study are listed in Table SI.

Western blot analysis. Protein extracts were obtained from human gastric cancer cell lines AGS and MKN-45 using RIPA lysis buffer (Promega Corporation). Protein concentrations were determined using the Pierce BCA Protein Assay Kit (cat. A55865; Invitrogen™; Thermo Fisher Scientific, Inc.). Subsequently, 30 μg aliquots of protein from each sample were subjected to SDS-PAGE on 12% Bis-Tris polyacrylamide gels, and the separated protein products were transferred onto 0.45-μm polyvinylidene fluoride membranes. The membranes were blocked with 5% skimmed milk (Beyotime Institute of Biotechnology) at room temperature for 1 h and incubated with primary antibodies for 4 h at 4˚C, followed by incubation with secondary antibodies for 1 h at room temperature. Protein levels were normalized against those of β-actin. The primary antibodies used in the present study included the following: CIAO1 (1:1,000; cat. no. 10295-1-AP; Proteintech Group, Inc.), FDX1 (1:1,000; cat. no. 12592-1-AP; Proteintech Group, Inc.), LIAS (1:1,000; cat. no. 11577-1-AP; Proteintech Group, Inc.) and β-actin (1:20,000; cat. no. 66009-1-Ig; Proteintech Group, Inc.). The secondary antibodies were HRP-conjugated goat anti-rabbit IgG (1:5,000; cat. no. GB23303) and HRP-conjugated

goat anti-mouse IgG (1:5,000; cat. no. GB23301; both Wuhan Servicebio Technology Co., Ltd.). Detection of chemiluminescence was performed using an ECL chemiluminescence substrate (Jiangsu Keygen Biotech Co., Ltd.), and protein bands were visualized using an imaging system (cat. no. A44116; Invitrogen; Thermo Fisher Scientific, Inc.) (25).

Gene knockdown studies. Oligonucleotides encoding short hairpin (sh)RNAs targeting CIAO1 were sourced from Merck KGaA. The shRNA sequences were subcloned into the GV298 vector (cat. no. GCD0316554; Shanghai Genechem Co., Ltd.), with 2 μg nucleic acid. Transfections were performed using the CHO Transfection Kit (cat. no. A29129; Invitrogen™; Thermo Fisher Scientific, Inc.), conducted at 37˚C for 24 h. Following transfection, AGS and MKN-45 cells were cultured for 24 h. The sequences of the oligonucleotides are listed in Table SII. Stable human gastric cancer cell lines AGS and MKN-45 expressing the shRNAs were subsequently selected through antibiotic resistance, employing puromycin (cat. no. A1113803; Invitrogen™; Thermo Fisher Scientific, Inc.) at cell line-specific concentrations: 2.0 μg/ml for AGS and 1.5 μg/ml for MKN-45 during initial selection (7-day treatment), followed by maintenance at 0.5 μg/ml for both lines (26).

MTT assay. Human gastric cancer AGS and MKN-45 cells were seeded into 96-well plates at a density of 5,000 cells per well (with five replicates per group), before being stably transfected with sh-scramble (scb), sh-CIAO1 #1 or sh-CIAO1 #2 vectors. After a 48-h incubation period at 37˚C, 20 μl MTT solution was added to each well, and the plates were incubated at 37˚C for a further 4 h. Subsequently, the medium (Ham's F12K) was removed, and DMSO was added to solubilize the formed formazan crystals. The absorbance was then immediately measured at 490 nm using an microplate reader (cat. VLBL00GD2; Invitrogen™; Thermo Fisher Scientific, Inc.), and the average absorbance for each group was subsequently calculated (27).

Soft agar assay. A total of $6x10^3$ cells (AGS and MKN-45) were suspended in 0.3% Noble Agar (Thermo Fisher Scientific, Inc.) and layered on to a base of 0.6% solidified agar in Ham's F12K medium supplemented with 10% FBS in 6-well plates. Following a 3-week incubation period (37˚C), the cells were fixed with 100% methanol for 20 min at room temperature and stained with 0.5% crystal violet dye for 30 min at room temperature. After staining, the cells were visualized using a light microscope (28).

Transwell assay. A 24-well plate was prepared with 500 μl DMEM per well, and Transwell inserts were precoated with 50 μl Matrigel (cat. no. G4130-5ML; Wuhan Servicebio Technology Co., Ltd.) at 4˚C for 30 min before being placed into the wells containing Ham's F12K. Following trypsinization, cells (human gastric cancer cell lines AGS and MKN-45) were centrifuged at 1,200 x g) for 5 min at room temperature, then resuspended and counted. A serum-free cell suspension at an appropriate concentration (10,000 cells per well) was prepared and added to each upper Transwell insert. A total of three replicates were set up for each group. The incubation was performed at 37˚C for 24 h. Medium was discarded and the cells were fixed with 100% methanol for 20 min at room temperature before being stained with crystal violet for 30 min at room temperature. Non-invading cells in the upper chambers were carefully removed using cotton swabs. Images of invaded cells on the lower membrane surface were captured using a fluorescent microscope, and the number of cells was counted. For quantification, images of nine random fields per insert were captured at identical magnification and analyzed using the latest version (1.53k) of ImageJ software (National Institutes of Health) (29).

Immunofluorescence assay. Human gastric cancer cell lines AGS and MKN-45 were cultured on coverslips, fixed with 4% paraformaldehyde for 20 min at room temperature, blocked with 5% milk for 1 h at room temperature and incubated overnight at 4˚C with antibodies specific for CIAO1 (1:200, cat. no. 10295-1-AP; Proteintech, Group, Inc.). Subsequently, coverslips were treated with Alexa Fluor 594-conjugated goat anti-rabbit IgG (1:1,000; cat. no. ab150160; Abcam) for 1 h at room temperature, followed by staining with 300 nmol/l DAPI (cat. no. D9542; Sigma-Aldrich; Merck KGaA) for 15 min at room temperature. Finally, images were captured using a Nikon A1Si laser-scanning confocal microscope (Nikon Corporation) (30).

Statistical analysis. The bioinformatics data were analyzed using R software (version 4.2.1, The R Foundation), SangerBox (version 3.0) (31) and Microinformatics (bioinformatics.com.cn/). For the experimental data obtained from basic research, statistical analysis was conducted using GraphPad Prism 9.0 (Dotmatics). Data are presented as the mean ± SD (n=3). For parametric comparisons between two groups, either unpaired or paired two-tailed Students' t-tests were performed, depending on the experimental design. For non-parametric comparisons between two groups, the Wilcoxon rank-sum test was applied. Moreover, the Pearson correlation coefficient test was used for assessing linear relationships between variables. For comparisons involving ≥3 groups meeting non-parametric assumptions, the Kruskal-Wallis test was employed, followed by Dunn's post hoc test. Clinicopathological characteristics between the training and testing datasets were analyzed using the χ^2 test or Fisher's exact test, as appropriate. $P<0.05$ was considered to indicate a statistically significant difference.

Results

Development of a risk model based on CRGs in TCGA dataset. A cohort of 348 patients with STAD were selected from TCGA database for the present study, as in Fig. 1. Transcriptome data identified a total of 22,628 differentially expressed genes (DEGs) through a comparison of gene expression levels between gastric cancer tissues and adjacent normal tissues. These were subsequently visualized using a volcano plot ($P<0.05$ and $|\log_2 FoldChange\ (FC)|>0.585$; Fig. 2A). Through intersecting these DEGs with genes associated with cuproptosis, a total of 41 differentially expressed CRGs (DE-CRGs) were identified (Fig. 2B). The 348 patients with STAD were randomly

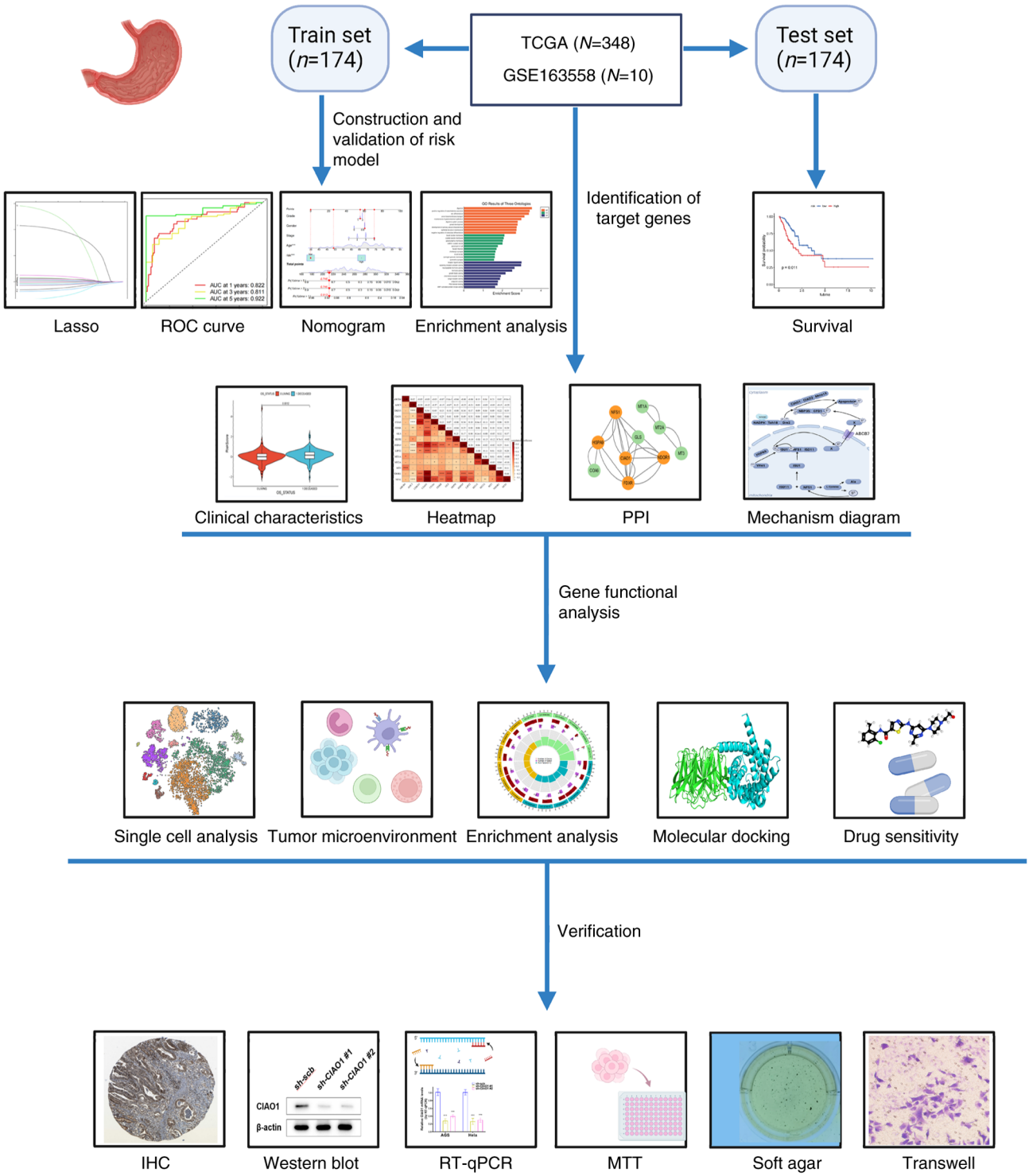

Figure 1. Schematic workflow of the development and validation of the risk model using TCGA, highlighting key genes and their interaction mechanisms through gene expression analysis, survival curve plotting and network diagram construction. Potential drug targets were identified, and their efficacy was assessed using *in vitro* experiments. TCGA, The Cancer Genome Atlas; LASSO, Least absolute shrinkage and selection operator; ROC, receiver operating characteristic; PPI, protein-protein interaction; IHC, immunohistochemistry; RT-qPCR, reverse transcription-quantitative PCR.

assigned to either a training or a testing cohort. No significant differences in clinical characteristics were observed between these two groups (Table I). Multivariate Cox regression analysis pinpointed 18 prognosis-associated CRGs. Furthermore, LASSO regression analysis was utilized to construct a risk model comprising a 15-gene signature (Fig. 2C and D). Of these genes, six were demonstrated to perform roles in the assembly of Fe/S proteins, whereas the remaining five were revealed to be associated with metallothionein-binding metals. The risk model score was determined as follows:=(ABCB4 x 0.387)+(AOC3 x 0.004) + CDKN3 x 0.014)+(CIAO1 x 0.005)+(COA6 x 0.02)-(FDXR x 0.016)+(GLS x 0.02)-(HEPH x 0.009)+[heat-shock protein (HSP)A9 x 0.006]+(LIPT2 x 0.034)-(MT1A x 0.043)+(MT2A x 0.003)+(MT3 x 0.395)-(NDOR1 x 0.053)-

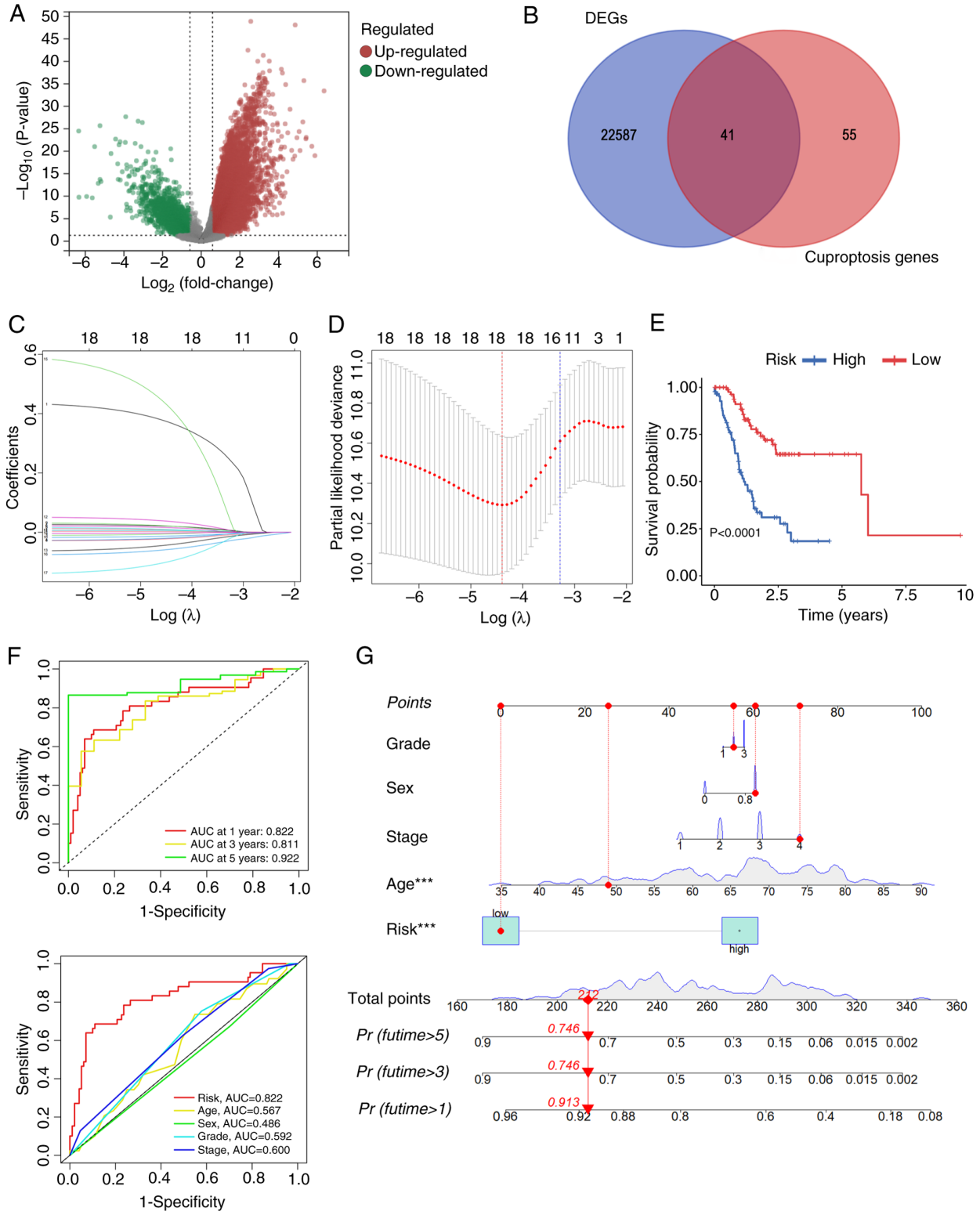

Figure 2. Development of a risk model based on CRGs in TCGA dataset. (A) A volcano plot was constructed to identify genes exhibiting differential expression between tumor and normal tissues (|Log FoldChangel>0.585; P<0.05). (B) Venn diagram showing 41 DEGs from TGCA-STAD. (C) Least absolute shrinkage and selection operator coefficient profile. (D) Optimal λ selection via cross-validation. (E) Survival differences between high- and low-risk groups were analyzed in the training cohort. (F) AUC values for 1-, 3- and 5-year survival rates. Receiver operator characteristic curves were constructed for the different clinical characteristics, and a risk model was developed. (G) Nomogram was constructed to predict overall survival rates at 1, 3 and 5 years for patients with gastric cancer. ***P<0.001. TCGA, The Cancer Genome Atlas; DEGs, differentially expressed genes; STAD, stomach adenocarcinoma; CRGs, cuproptosis-related genes; AUC, areas under the receiver operating characteristic curves.

[nitrogen fixation 1 (NFS1) x 0.082]. Kaplan-Meier survival curves demonstrated that patients with STAD who had lower risk scores exhibited significantly improved overall survival (OS) rates compared with those with higher risk scores (Figs. 2E and S1). Additionally, the survival rates at 1, 3 and 5 years, determined by the risk scores of the DE-CRGs, were

Table I. Clinical features of patients with gastric adenocarcinoma.

Covariate	Total (n=346)	Testing group (n=172)	Training group (n=174)	P-value
Age				
≤65 years	157 (45.38)	84 (48.84)	73 (41.95)	0.2177
>65 years	186 (53.76)	86 (50.00)	100 (57.47)	
Unknown	3 (0.87)	2 (1.16)	1 (0.57)	
Sex				
Female	122 (35.26)	68 (39.53)	54 (31.03)	0.1230
Male	224 (64.74)	104 (60.47)	120 (68.97)	
Grade				
G1	8 (2.31)	3 (1.74)	5 (2.87)	0.7693
G2	123 (35.55)	62 (36.05)	61 (35.06)	
G3	206 (59.54)	104 (60.47)	102 (58.62)	
Unknown	9 (2.60)	3 (1.74)	6 (3.45)	
Stage				
I	45 (13.01)	26 (15.12)	19 (10.92)	0.2501
II	110 (31.79)	51 (29.65)	59 (33.91)	
III	143 (41.33)	67 (38.95)	76 (43.68)	
IV	34 (9.83)	21 (12.21)	13 (7.47)	
Unknown	14 (4.05)	7 (4.07)	7 (4.02)	
T stage				
T1	15 (4.34)	8 (4.65)	7 (4.02)	0.8215
T2	74 (21.39)	37 (21.51)	37 (21.26)	
T3	158 (45.66)	74 (43.02)	84 (48.28)	
T4	95 (27.46)	50 (29.07)	45 (25.86)	
Unknown	4 (1.16)	3 (1.74)	1 (0.57)	
N stage				
N0	102 (29.48)	42 (24.42)	60 (34.48)	0.1057
N1	91 (26.30)	53 (30.81)	38 (21.84)	
N2	71 (20.52)	38 (22.09)	33 (18.97)	
N3	71 (20.52)	34 (19.77)	37 (21.26)	
Unknown	11 (3.18)	5 (2.91)	6 (3.45)	
M stage				
M0	309 (89.31)	156 (90.70)	153 (87.93)	0.5174
M1	22 (6.36)	9 (5.23)	13 (7.47)	
Unknown	15 (4.34)	7 (4.07)	8 (4.60)	

Data are presented as n (%). T, tumor; N, node; M, metastasis.

reflected by areas under the ROC curve (AUC) values of 0.822, 0.811 and 0.922, respectively, indicating high sensitivity and specificity (Fig. 2F). ROC curves were subsequently generated to evaluate clinically relevant factors, and this analysis revealed that the risk score was the most valuable prognostic predictor when compared with other clinical features, such as age, sex, grade and tumor stage (Fig. 2F). To estimate the 1-, 3- and 5-year OS rates of patients with STAD, a nomogram was constructed that included the clinical characteristics of grade, sex, age, stage and risk score (Fig. 2G). Collectively, these analyses demonstrated that, based on the CRGs, the developed risk model exhibited independent and reliable values in terms of predicting the prognosis of patients with STAD.

Clinical characteristics and functional enrichment of high- and low-risk groups of the CRG model. To further assess the potential impact of risk scores on patients with STAD, the DEGs between these two groups with a significance threshold of $P<0.05$ and $|\log2\ FC|>1$ were identified (Fig. S2A). Gene set enrichment analysis (GSEA) revealed that these DEGs were primarily involved in base-excision repair, one-carbon pool by folate or pantothenate and CoA biosynthesis (Fig. S2B). GO enrichment analysis indicated that these DEGs were primarily associated with digestion, brush border membrane and receptor ligand activity in the high- vs. low-risk groups (Fig. S2C). KEGG pathway enrichment analysis demonstrated that these genes were significantly associated with 'cAMP

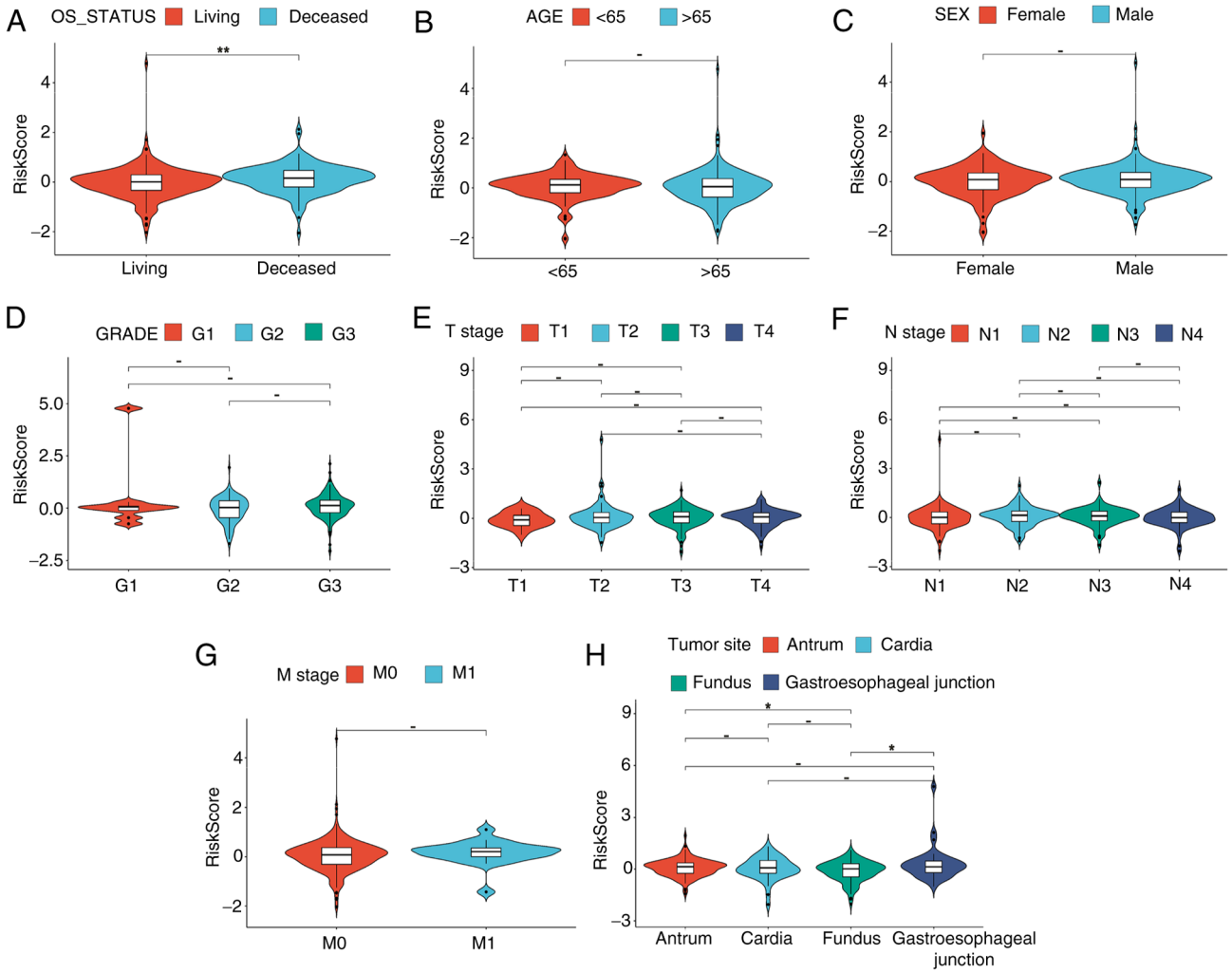

Figure 3. Clinical characteristics of high- and low-risk groups of the cuproptosis gene-associated model. The associations between the risk score derived from the cuproptosisassociated gene model and several clinical characteristics of patients with gastric cancer were determined. The risk score was used to stratify patients into high- and low-risk groups, and its association with key clinical parameters was analyzed. (A) OS status; (B) age; (C) sex; (D) grade; (E) T stage; (F) N stage; (G) M stage; and (H) primary site of patients with gastric cancer. *P<0.05; **P<0.01. OS, overall survival; T, tumor; N, lymph node; M, metastasis.

signaling pathway', 'pancreatic secretion' and bile secretion (Fig. S2D).

Furthermore, a strong association between risk score and several of the clinical characteristics of patients with STAD was demonstrated. Notably, the risk scores of deceased patients were revealed to be significantly higher compared with those of survivors (P<0.05; Fig. 3A). Additionally, in terms of the primary tumor site, the risk scores for cancers located at the gastroesophageal junction or antrum/distal part of stomach were revealed to be significantly higher compared with those of the fundus/body (P<0.05; Fig. 3H). However, the analysis did not demonstrated any significant differences in risk scores for different subtypes based on parameters such as age, sex, grade, T stage, N stage or M stage (Fig. 3B-G). These results suggest that patients with worse outcomes have higher risk scores in the CRG model.

Elevated CIAO1 expression is crucial for the assembly of Fe/S clusters in STAD. A correlation heatmap was generated to illustrate the correlations among these risk model signature genes (Fig. 4A). The protein-protein interaction (PPI) networks were obtained from the STRING database (Fig. 4B). To assess the importance of individual genes in 32 gastric cancer cell lines, public gene knockout datasets generated using CRISPR-Cas9 technology were obtained from the iCSDB (icsdb.lk/) database, which indicated that *HSPA9*, *NFS1* and *CIAO1* were the genes essential for the viability of gastric cancer cells (Fig. 4C). Based on its known functions, described in the existing literature, *CIAO1*, an essential gene involved in the assembly of Fe/S proteins and strongly associated with other genes (32) (Fig. 4D), was chosen for further investigation. Kaplan-Meier survival curve analysis revealed that patients with gastric cancer with elevated levels of *CIAO1* had a worse prognosis than those with a low expression of *CIAO1* (Fig. 4E). Furthermore, differential analysis demonstrated that the level of *CIAO1* expression was significantly higher in STAD tissues compared with that in normal tissues (Fig. 4F). Moreover, through mining the Human Protein Atlas (HPA) database (https://www.proteinatlas.org/), immunohistochemistry staining data for the CIAO1 protein indicated that its primary localization was within the cytoplasm, with a markedly stronger staining intensity in gastric cancer tissues

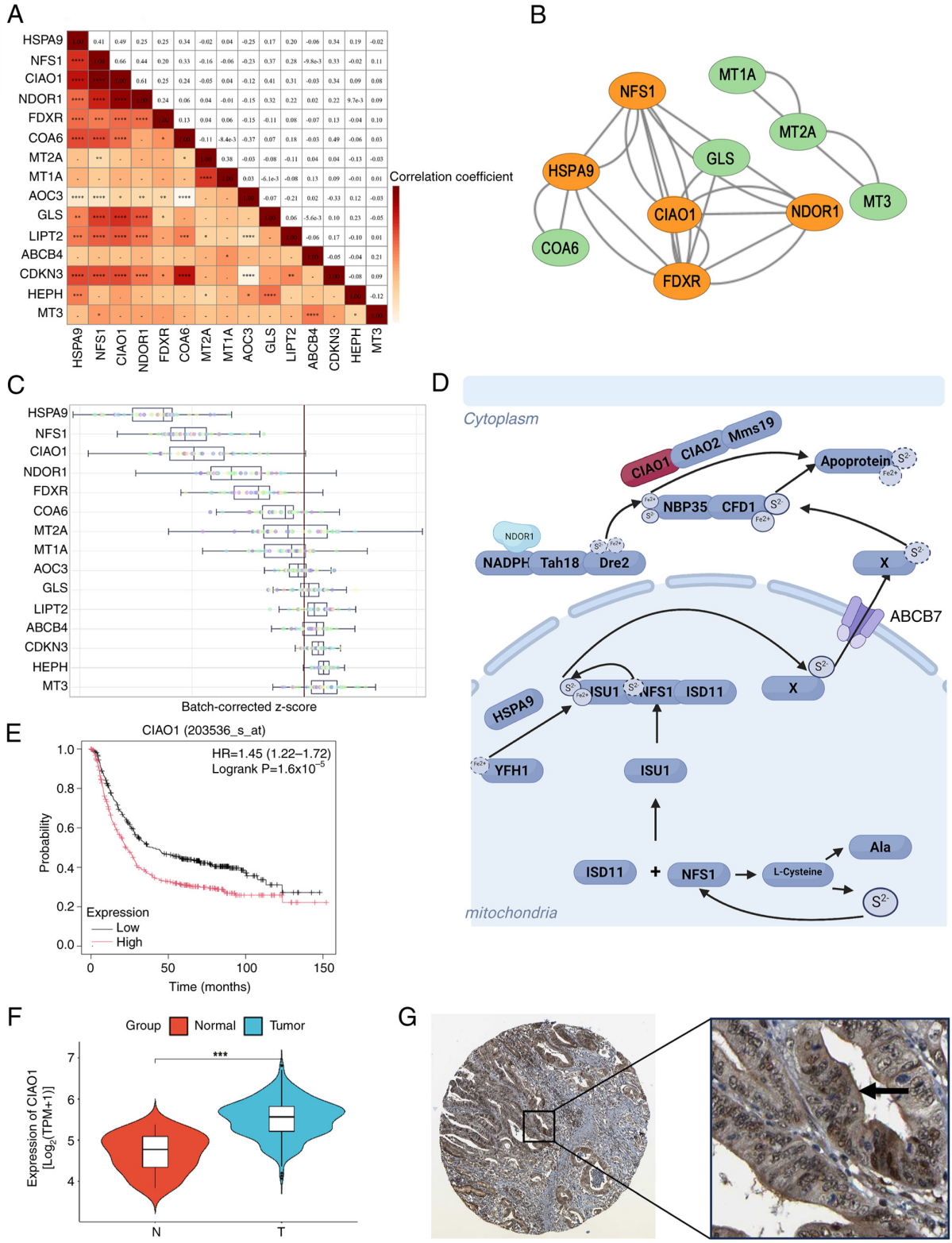

Figure 4. Elevated *CIAO1* expression is crucial for assembly of iron-sulfur clusters in stomach adenocarcinoma. (A) Heatmap illustrating the correlation among 15 DE-CRGs. (B) Protein-protein interaction network plot of 15 DE-CRGs. (C) Box plot illustrating the z-score of the 15 DE-CRGs. (D) Mechanism of the iron-sulfur cluster assembly process. (E) Survival analysis of patients with gastric cancer with high or low *CIAO1* levels, determined using the Kaplan-Meier Plotter database. (F) *CIAO1* gene expression in gastric cancer tissues compared with adjacent normal tissues. *P<0.05, **P<0.01, ***P<0.001, ****P<0.0001. (G) Immunohistochemical staining of CIAO1 in gastric cancer tissue. Magnification, x40 times (left) and 400 times (right) respectively). CIAO1, cytosolic ironsulfur assembly component 1; DE-CRGs, differentially expressed cuproptosis-related genes; HR, hazard ratio; N, lymph node; T, tumor; TPM, transcripts per million.

compared with that in noncancerous tissues (Fig. 4G). Taken together, these data indicate that an increased level of CIAO1 is crucial for the assembly of Fe/S clusters in STAD.

CIAO1 expression is associated with clinicopathological features of STAD. To further evaluate the association between *CIAO1* expression and the prognosis of patients

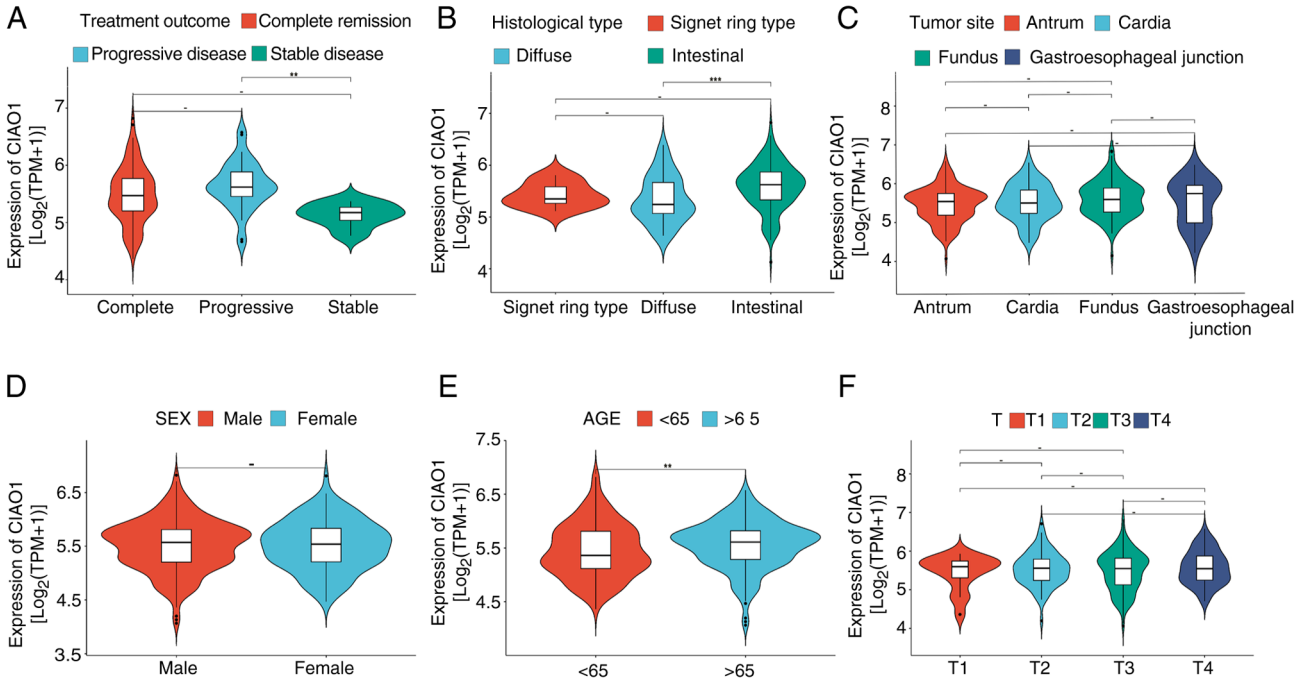

Figure 5. *CIAO1* expression is associated with clinicopathological features of stomach adenocarcinoma. The association between the *CIAO1* expression levels and several clinicopathological characteristics of patients with gastric cancer were determined, providing insights into the potential role of *CIAO1* in tumor progression and patient outcomes. (A) Treatment outcome; (B) histological type; (C) tumor site; (D) sex; (E) age; and (F) T stage of patients with gastric cancer. **P<0.01; ***P<0.001. *CIAO1*, cytosolic iron-sulfur assembly component 1; TPM, transcripts per million; T, tumor.

with STAD, expression data and clinical information from TCGA database were analyzed. From a treatment efficacy perspective, *CIAO1* expression was revealed to be significantly higher in patients who experienced progressive disease after the first course of treatment, compared with those who achieved complete remission/response and stable disease (Fig. 5A). From a histological standpoint, *CIAO1* expression was significantly elevated in the intestinal type of STAD compared with the diffuse type (Fig. 5B). In terms of age stratification, the expression level of *CIAO1* in older patients was significantly higher than that in younger patients (Fig. 5E). However, there was no significant difference in *CIAO1* expression among subgroups stratified by sex, primary tumor site or T stage (Fig. 5C, D and F). Considered altogether, the aforementioned results suggest that *CIAO1* expression is associated with clinicopathological features of STAD.

Impact of CIAO1 expression on the tumor microenvironment and immune-related markers in STAD. The distribution of *CIAO1* in patients with STAD was subsequently assessed using the single-cell RNA sequencing dataset, GSE163558. Annotation of principal cell types within these datasets revealed that *CIAO1* expression was markedly higher in tumor cells compared with other cell types (Figs. 6A and B, and S3). Additionally, analyses were performed to detect differences in other significant characteristics among the several groups. The expression levels of immune checkpoints were specifically assessed, revealing the presence of significantly higher levels of *prephenate dehydratase 1*, *programmed cell death 1 ligand 2*, *cytotoxic T-lymphocyte associated protein 4*, *CD80*, *CD86*, *lymphocyte activating 3*, *hepatitis A virus cellular receptor 2*, *CEA cell adhesion molecule 1* and *signal regulatory protein α* in the high *CIAO1* expression group compared with the low expression group (Fig. 6C). Furthermore, the group with elevated *CIAO1* expression exhibited a TMB, indicating a stronger immune response compared with the lower expression group (Fig. 6D). To evaluate tumor microenvironment differences, ESTIMATE scores were calculated for the samples. The results obtained demonstrated that the high *CIAO1* expression group had significantly lower ESTIMATE scores compared with the low expression group (Fig. 6E). Additionally, this high expression group exhibited significantly lower immune and stromal scores, whereas tumor purity was significantly higher, compared with the low expression group (Fig. S4). Taken together, these findings indicate that *CIAO1* expression is associated with treatment outcomes, histological type, immune checkpoint expression, TMB and the tumor microenvironment in patients with gastric cancer.

Enrichment analysis of DEGs and CIAO1-interacting proteins in STAD. To assess the cellular functions influenced by *CIAO1*, a volcano plot was used to visualize 368 DEGs between the high- and low-*CIAO1* expression groups within TCGA database (P<0.05; |log2FC|>1; Fig. 7A). GO enrichment analysis revealed that these DEGs were mainly associated with chromosome segregation, spindle function and microtubule motor activity (Fig. 7B). Furthermore, GSEA revealed that these DEGs were predominantly associated with the cell cycle, pyruvate metabolism and metabolism of alanine, aspartate and glutamate (Fig. 7C). The STRING database was subsequently used to evaluate the PPIs involving CIAO1, resulting in the construction of a

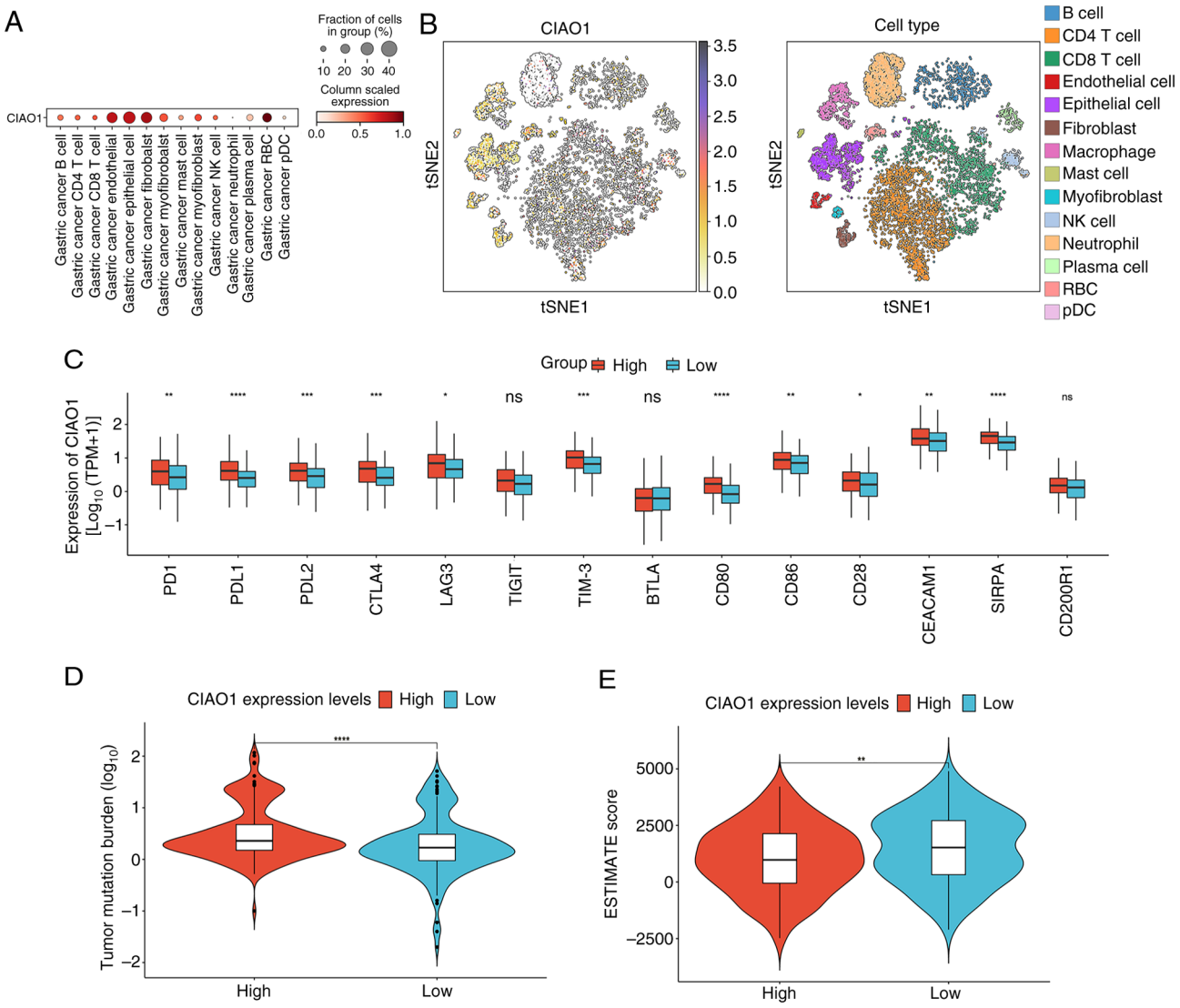

Figure 6. Impact of *CIAO1* expression on the tumor microenvironment and immune-associated markers in stomach adenocarcinoma. (A) Expression and distribution of CIAO1 across cell types in gastric cancer. (B) t-SNE plots were used to visualize the distribution of CIAO1 in cell subtypes in the three patients with gastric cancer. Expression levels of (C) immune checkpoints, (D) tumor mutation burden and (E) ESTIMATE scores, comparing the high- and low-*CIAO1* expression groups. *P<0.05; **P<0.01; ***P<0.001; ****P<0.0001. *CIAO1*, cytosolic iron-sulfur assembly component 1; tSNE, t-distributed stochastic neighbor embedding; NK, natural killer; RBC, red blood cell; pDC, plasmacytoid dendritic cell; TPM, transcripts per million; *PD1*, prephenate dehydratase 1; *PDL2*, programmed cell death 1 ligand 2; *CTLA4*, cytotoxic T-lymphocyte associated protein 4; *LAG3*, lymphocyte activating 3; *HAVCR2*, hepatitis A virus cellular receptor 2; *CEACAM1*, carcinoembryonic antigen-related cell adhesion molecule 1; *SIRPA*, signal regulatory protein α; ns, not significant.

network diagram to illustrate these interactions. This analysis revealed that CIAO1 predominantly interacts with proteins such as NUBP Fe/S cluster assembly factor 2, cytosolic, DNA polymerase delta 1 catalytic subunit, ERCC excision repair 2 TFIIH core complex helicase subunit, MMS19, solute carrier family 25 members 5 and 6, CIAO2A and CIAO3 (Fig. 7D). Moreover, KEGG pathway enrichment analysis revealed that these DEGs were significantly associated with the cell cycle, motor proteins and the Fanconi anemia pathway (Fig. 7E). The threedimensional structures of CIAO1 and its interacting proteins were obtained from the UniProt database. Utilizing the HDOCK program (http://hdock.phys.hust. edu.cn/), molecular docking studies were then performed on these proteins and the optimal docking model was selected for further analysis. PyMOL was used to visualize these interactions (Figs. 7F-H and S5). These comprehensive analyses indicate potential molecular mechanisms through which CIAO1 may influence cellular processes in STAD.

Identification of transcriptional inhibitors of CIAO1 expression. To assess potential therapeutic effects of different drugs on CIAO1 expression, the IC_{50} values of drugs were calculated using the R package 'pRRophetic'. An initial screening identified 563 drugs, of which 318 were in clinical trials and received FDA approval. The results demonstrated that treatment with the drugs nelarabine, cladribine, nitazoxanide, fludarabine, masoprocol, econazole nitrate, methylprednisolone, ZM336372, idebenone or vorinostat was positively associated with the expression of CIAO1. By contrast, the drugs that were negatively correlated with CIAO1 were dasatinib and AT-9283 (Fig. 8). These data suggest that these two drugs may potentially be suitable as transcriptional inhibitors of CIAO1 expression.

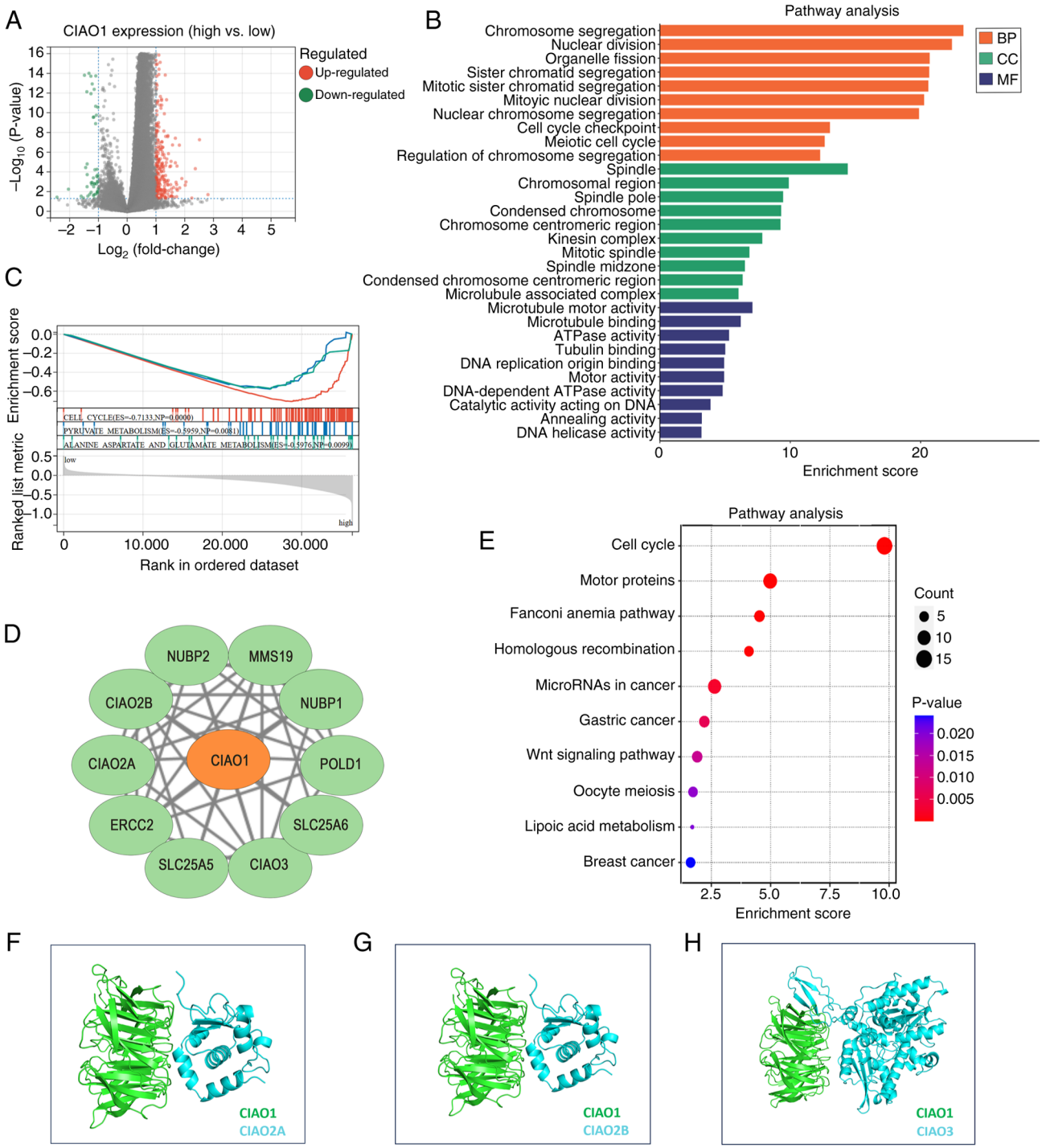

Figure 7. Enrichment analysis of DEGs and CIAO1-interacting proteins in stomach adenocarcinoma. (A) Volcano plot, highlighting the DEGs between the high- and low-*CIAO1* expression groups [Log(FoldChange)<1; P<0.05]. (B) Gene Ontology functional enrichment analysis for DEGs. (C) Geneset enrichment analysis. (D) Protein-protein interaction network plot of CIAO1-interacting proteins. (E) Kyoto Encyclopedia of Genes and Genomes functional enrichment analysis for DEGs. The three-dimensional visualization of the structure of CIAO1 and its interacting proteins: (F) CIAO2A, (G) CIAO2B and (H) CIAO3. DEGs, differentially expressed genes; CIAO, cytosolic iron-sulfur assembly component; BP, Biological Process; CC, Cellular Compartment; MF, Molecular Function.

Pharmacological inhibition of CIAO1 induces cuproptosis and inhibits the aggressiveness of cancer cells. The protein levels of CIAO1 were detected in several human cell lines, including GES-1, AGS, SNU-1, MKN-45, HGC-27, 293 and HeLa cell lines (Fig. 9A). Among the selected cell lines, AGS and MKN-45, which exhibit higher CIAO1 expression in gastric cancer cells, were chosen as model systems for further investigation. Additionally, to evaluate the functional role of CIAO1 in other cancer types, complementary experiments were performed using the HeLa cell line. Gastric cancer (AGS and MKN-45) and HeLa cells with *CIAO1* knocked-down were established, and the knockdown of *CIAO1* was assessed using RT-qPCR (Figs. 9B and S6A). The RT-qPCR results revealed that the knockdown efficiencies of the two sequences

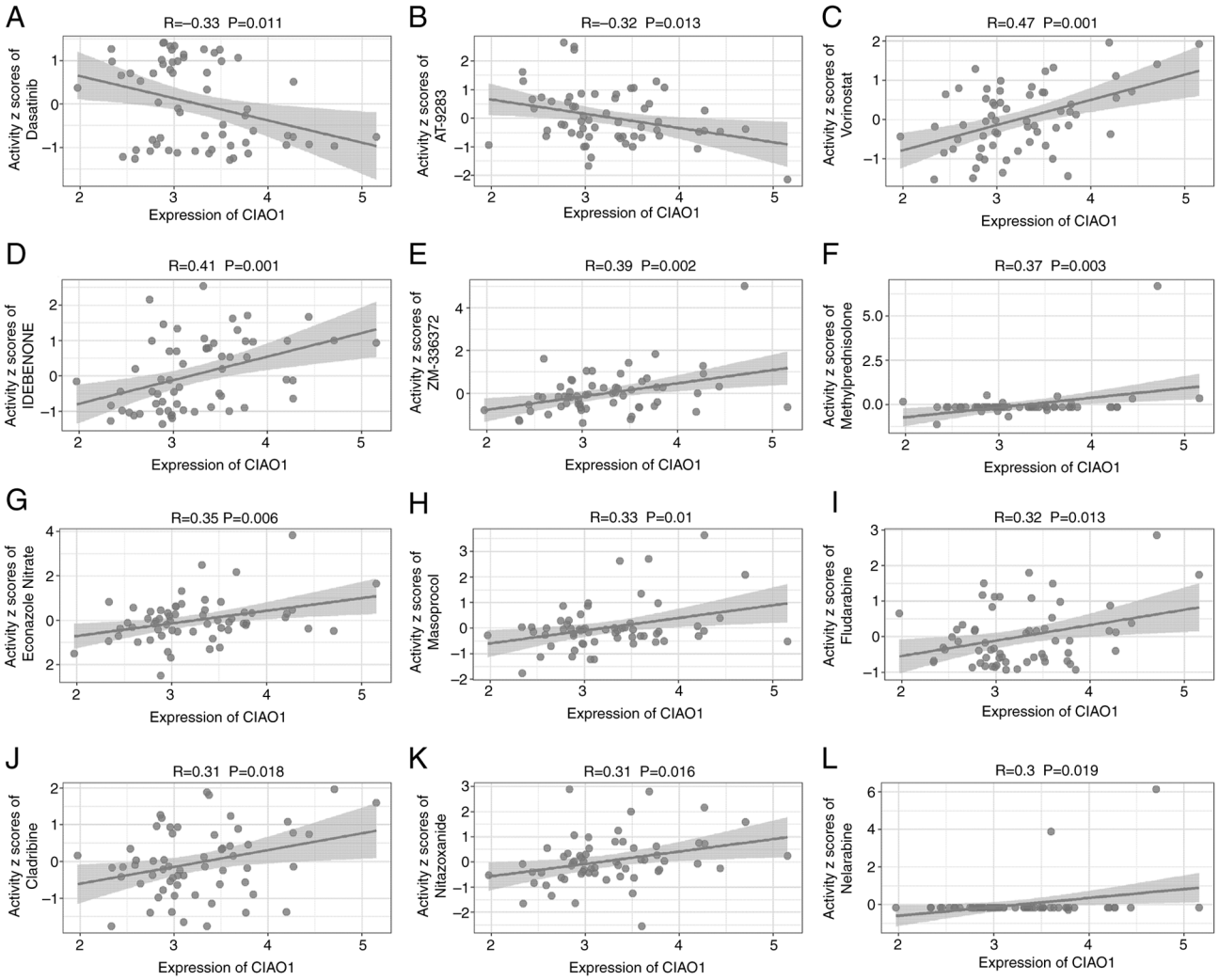

Figure 8. Identification of transcriptional inhibitors of *CIAO1* expression. Drug sensitivity assessments for (A) dasatinib, (B) AT-9283, (C) vorinostat, (D) idebenone, (E) ZM-336372, (F) methylprednisolone, (G) econazole nitrate, (H) masoprocol, (I) fludarabine, (J) cladribine, (K) nitazoxanide and (L) nelarabine on *CIAO1* transcript levels. *CIAO1*, cytosolic ironsulfur assembly component 1.

were similar, both effectively reducing *CIAO1* expression to a comparable extent. Therefore, both knockdown approaches were utilized in subsequent experiments to ensure consistent validation. As an excessive amount of copper ions directly interact with lipoylated proteins in the tricarboxylic acid cycle, causing their aggregation and the degradation of Fe/S cluster proteins (6), and also in view of the fact that there is evidence to suggest that HSP70 is a heat-shock protein that triggers the proteotoxic stress response during copper death (or cuproptosis) (33,34), FDX1 or LIAS (as Fe/S cluster proteins) and HSP70 were selected as biomarkers of copper-induced cytotoxicity. Notably, the western blot analysis experiments revealed a marked decrease in the protein levels of FDX1 and LIAS, but an increase in the expression levels of HSP70 following CIAO1 knockdown in AGS, MKN-45 and HeLa cell lines (Figs. 9C and S6B). Moreover, immunofluorescence demonstrated that localization of CIAO1 was observed in the nucleus and cytosol of the AGS, MKN-45 and HeLa cells (Figs. 9D and S6C). CIAO1 knockdown was also associated with a notable reduction in the fluorescence intensity of CIAO1. Furthermore, treatment with the CIAO1 inhibitors dasatinib and AT-9283 markedly reduced the expression of CIAO1 and the Fe/S cluster proteins (FDX1 and LIAS), but led to an increase in the levels of HSP70 (Figs. 9E and S6D). MTT colorimetric, soft agar and Matrigel invasion assays also revealed significant reductions in the viability, proliferation and invasion rates of AGS, MKN-45 and HeLa cells following stable *CIAO1* knockdown (Figs. 9F, H and I and S6E, G and H). Moreover, MTT colorimetric assays demonstrated significant reductions in the viability of AGS, MKN-45 and HeLa cells following treatment with Dasatinib or AT-9283 (Figs. 9G and S6F). Taken together, these results suggest that pharmacological inhibition of *CIAO1* both induces cuproptosis and inhibits the aggressiveness of cancer cells.

Discussion

The present study successfully constructed a prognostic model for gastric cancer based on CRGs. Through multiple analysis and screening, it was revealed that *CIAO1* is a key gene in the occurrence and development of gastric cancer. Previous studies have reported that *CIAO1* is not only significantly associated with poor prognosis in patients, but also serves a key role in regulating goblet apoptosis by regulating the assembly of Fe/S

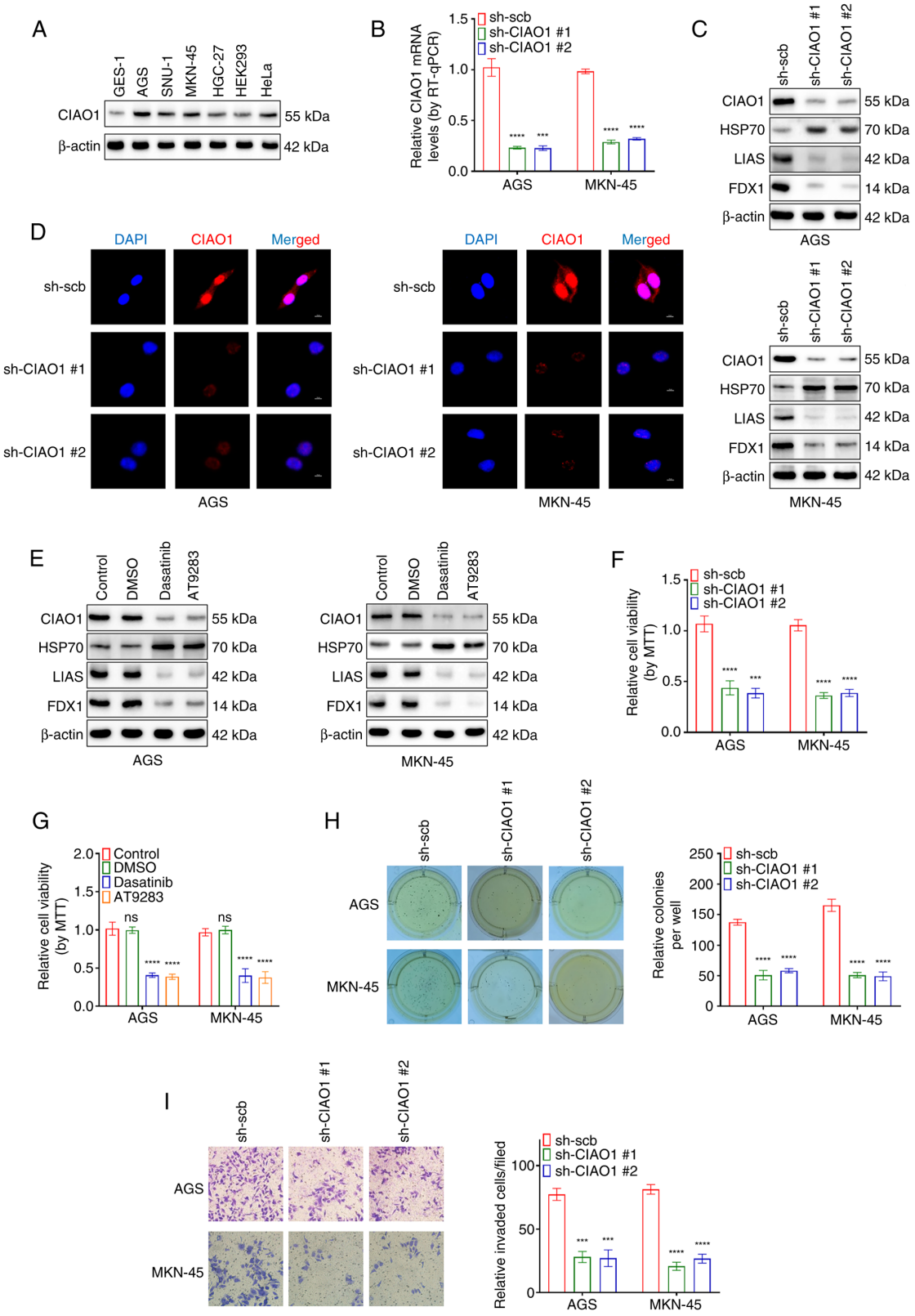

Figure 9. Pharmacological inhibition of CIAO1 induces cuproptosis and inhibits the aggressiveness of cancer cells. (A) Western blot analysis revealed the expression of CIAO1 in GES 1, AGS, SNU 1, MKN 45, HGC 27, HEK293 and HeLa cell lines. (B) RT-qPCR assays (normalized to βactin) demonstrated the *CIAO1* expression levels, (C) western blot analysis revealed the CIAO1, FDX1, LIAS and HSP70 expression levels and (D) immunofluorescence assays demonstrated the localization and fluorescence intensity of CIAO1 expression (scale bar, 10 μm) in AGS and MKN-45 cells transfected with sh-Scb, sh-*CIAO1* #1 or sh-*CIAO1* #2. (E) Western blot analysis revealed the CIAO1, FDX1, LIAS and HSP70 expression levels in AGS and MKN-45 cells treated with dasatinib (0.5 nmol/l) or AT-9283 (4 nmol/l). MTT colorimetric assays demonstrated changes in the viability of AGS and MKN-45 cells (F) transfected with sh-Scb, sh-*CIAO1* #1 or sh-*CIAO1* #2 and (G) treated with dasatinib (0.5 nmol/l) or AT9283 (4 nmol/l). Representative images (left panels) and quantification of the data (right panels) of (H) soft agar and (I) Matrigel invasion assays, demonstrated the anchorage-independent proliferation and invasion of AGS and MKN-45 cells stably transfected with sh-Scb, sh-*CIAO1* #1 or sh-*CIAO1* #2. Magnification, x100. ***P<0.001; ****P<0.0001 vs. sh-Scb. *CIAO1*, cytosolic iron-sulfur assembly component 1; RT-qPCR, reverse transcription-quantitative PCR; sh, short hairpin; Scb, scramble; FDX1, ferredoxin 1; LIAS, lipoic acid synthetase; HSP70, heat shock protein 70; ns, not significant.

proteins (7,11). In addition, the present study demonstrated that dasatinib and AT-9283 can selectively inhibit its expression, highlighting the potential of *CIAO1* as a new target for gastric cancer treatment. However, the specific molecular mechanism of CIAO1 in the regulation of goblet apoptosis and its specific mechanism of involvement in other signaling pathways remain to be fully elucidated.

Despite the downward trend in the global incidence and mortality of gastric cancer (annual decrease of 1.5-2% in age-standardized rates, GLOBOCAN 2020-2022), which are mainly due to advances in immunotherapy (35,36), notable clinical challenges remain. For example, high microsatellite instability and Epstein-Barr virus positive subtypes are sensitive to programmed cell death protein 1/programmed death-ligand 1 inhibitors, whilst other subtypes have limited responses (37) and are prone to secondary drug resistance (38). Moreover, the high heterogeneity of the tumor immune microenvironment (39) requires the combination of multi-parameter flow cytometry, single-cell sequencing and high-throughput data analysis (40) to achieve accurate typing. Previous studies have reported that CRGs present marked expression heterogeneity in gastric cancer, and their expression pattern is closely associated with tumor immune escape, chemotherapy resistance and patient prognosis (1,10,41). These genes can affect the sensitivity of gastric cancer cells to copper death inducers by regulating copper ion homeostasis and mitochondrial function (10). In the present study, based on TCGA and GEO databases, 41 patients with gastric cancer with differential expression of CRGs were selected to construct a risk model. The results demonstrated that the 5-year survival rate of patients in the low-risk group was significantly higher than that in the high-risk group (AUC=0.922), and the risk score was significantly associated with primary site. However, the integration of traditional pathological markers with novel molecular markers (such as CRGs) remains the key to achieving dynamic and accurate assessment.

CIAO1 is expressed in several normal human tissues, although its specific expression level may vary depending on the tissue type. According to the data derived from the HPA database, it was revealed that *CIAO1* is expressed at higher levels in the parathyroid gland, liver, adrenal gland and kidney. According to the HPA database, *CIAO1* expression levels are notable increased in certain types of solid tumors, including ovarian cancer, gastric cancer and glioma (2,42). CIAO1, a fundamental component of the CIA complex (43), serves an essential role in incorporating Fe/S clusters into extramitochondrial Fe/S proteins (44,45). An absence of *CIAO1* may affect Fe/S cluster levels, which are crucial for cellular sensitivity to cuproptosis (46). A previous study revealed that deficiencies in *CIAO1* and *MMS19* led to impaired Fe/S cluster protein assembly, which, in turn, was associated with neurodegeneration (47). The present study further assessed the association between *CIAO1* expression and the prognosis of patients with gastric adenocarcinoma, the distribution of *CIAO1* in different cell types and the involvement of CIAO1 in cellular pathways. The results revealed that high levels of *CIAO1* expression are associated with a poor prognosis of patients with gastric cancer. *CIAO1* was primarily distributed in epithelial cells; therefore, we hypothesized that this may be associated with the active metabolism of epithelial tissues, and so additional Fe/S proteins would be required to serve a role. In this regard, the potentially negative regulatory effects of two drugs, dasatinib and AT-9283, on *CIAO1* expression were evaluated and the findings demonstrated that they may potentially provide novel therapeutic approaches. Dasatinib is a small-molecule tyrosine kinase inhibitor that exerts its antitumor effects through inhibiting multiple targets, including BCR-ABL kinase, and it has been widely used in the treatment of chronic myeloid leukemia and Philadelphia chromosome-positive acute lymphoblastic leukemia (48,49). AT-9283 is a multi-target small-molecule kinase inhibitor that has demonstrated notable antitumor activity in both hematological malignancies such as acute myeloid leukemia, acute lymphoblastic leukemia and lymphoma, and in solid tumors such as pancreatic cancer and non-small cell lung cancer, operating through a dual inhibitory mechanism involving the Aurora kinase and JAK signaling pathways (50). The present study demonstrated that both these drugs inhibit the proliferation and invasion of gastric cancer cells via reducing the expression of *CIAO1*, and these findings may provide an important basis for the further study of antitumor therapy.

Previous studies have reported that the occurrence of copper death is inseparable from protein toxicity stress responses and the reduction of Fe/S cluster proteins (3,6,51). Fe/S proteins fulfill important roles in cell metabolism and the mitochondrial electron transport chain, and reductions in their levels may markedly affect the function of mitochondria, leading to cell death (32). Therefore, the present study aimed to assess whether *CIAO1* was associated with the occurrence and development of copper death. To achieve this aim, cell experiments were performed, which revealed that when the expression level of *CIAO1* was decreased, the expression levels of the copper death markers FDX1 and LIAS were decreased, whereas those of HSP70 were increased, demonstrating the presence of higher levels of cellular copper death.

Despite the significant findings of the present study, several limitations should be acknowledged. First, the study primarily relied on bioinformatics analysis of publicly available datasets (TCGA and GEO databases); while validation experiments were conducted, further large-scale clinical trials are necessary to confirm these findings in diverse populations. Second, the CIAO1 knockdown experiments provided insights into the role of CIAO1 in Fe/S protein regulation and cuproptosis; however, its precise molecular interactions and upstream regulatory mechanisms, such as transcriptional regulation and epigenetic modifications, remain largely unexplored. Third, while dasatinib and AT-9283 were identified as potential inhibitors of CIAO1, their efficacy and safety in patients with gastric cancer patients have yet to be validated through preclinical and clinical studies. These limitations should be addressed in future studies to fully assess the therapeutic potential of CIAO1 and refine its role as a biomarker in gastric cancer.

In conclusion, the results of the present study demonstrated that *CIAO1* functions as a tumor-promoting factor in STAD. Elevated expression levels of *CIAO1* were revealed to be associated with a poor prognosis in patients with STAD. Moreover, it was demonstrated that CIAO1 may modulate the degree of cuproptosis in gastric cancer cells through regulating the expression levels of Fe/S cluster assembly proteins, thereby

influencing the proliferation and invasion rates of gastric cancer cells. Taken together, these findings suggest that *CIAO1* may serve as a potential therapeutic target, offering novel insights into the treatment of STAD.

Acknowledgements

Not applicable.

Funding

The present work was funded by the National Natural Science Foundation of China (grant nos. 82072801, 82173316, 82293663 and 82473092).

Availability of data and materials

The data generated in the present study are included in the figures and/or tables of this article.

Authors' contributions

JQ and LZ confirm the authenticity of all the raw data. LZ, QT and JQ conceived the study. JQ and CY analyzed and interpreted data and the cellular experiments. SZ and BZ analyzed the public datasets. LZ and QT supervised the study. All authors read and approved the final manuscript.

Ethics approval and consent to participate

Not applicable.

Patient consent for publication

Not applicable.

Competing interests

The authors declare that they have no competing interests.

References

1. Smyth EC, Nilsson M, Grabsch HI, van Grieken NC and Lordick F: Gastric cancer. Lancet 396: 635648, 2020.
2. Guan WL, He Y and Xu RH: Gastric cancer treatment: Recent progress and future perspectives. J Hematol Oncol 16: 57, 2023.
3. Joshi SS and Badgwell BD: Current treatment and recent progress in gastric cancer. CA Cancer J Clin 71: 264279, 2021.
4. Dicken BJ, Bigam DL, Cass C, Mackey JR, Joy AA and Hamilton SM: Gastric adenocarcinoma: Review and considerations for future directions. Ann Surg 241: 2739, 2005.
5. Ishida S, Andreux P, Poitry-Yamate C, Auwerx J and Hanahan D: Bioavailable copper modulates oxidative phosphorylation and growth of tumors. Proc Natl Acad Sci USA 110: 19507-19512, 2013.
6. Tsvetkov P, Coy S, Petrova B, Dreishpoon M, Verma A, Abdusamad M, Rossen J, JoeschCohen L, Humeidi R, Spangler RD, *et al*: Copper induces cell death by targeting lipoylated TCA cycle proteins. Science 375: 12541261, 2022.
7. Cobine PA and Brady DC: Cuproptosis: Cellular and molecular mechanisms underlying copper-induced cell death. Mol Cell 82: 1786-1787, 2022
8. Wang Y, Chen Y, Zhang J, Yang Y, Fleishman JS, Wang Y, Wang J, Chen J, Li Y and Wang H: Cuproptosis: A novel therapeutic target for overcoming cancer drug resistance. Drug Resist Updat 72: 101018, 2024.
9. Chen G, Luo D, Qi X, Li D, Zheng J, Luo Y, Zhang C, Ren Q, Lu Y, Chan YT, *et al*: Characterization of cuproptosis in gastric cancer and relationship with clinical and drug reactions. Front Cell Dev Biol 11: 1172895, 2023.
10. Chong W, Ren H, Chen H, Xu K, Zhu X, Liu Y, Sang Y, Li H, Liu J, Ye C, *et al*: Clinical features and molecular landscape of cuproptosis signature-related molecular subtype in gastric cancer. Imeta 3: e190, 2024.
11. Braymer JJ, Freibert SA, RakwalskaBange M and Lill R: Mechanistic concepts of ironsulfur protein biogenesis in biology. Biochim Biophys Acta Mol Cell Res 1868: 118863, 2021.
12. Srinivasan V, Netz DJ, Webert H, Mascarenhas J, Pierik AJ, Michel H and Lill R: Structure of the yeast WD40 domain protein Cia1, a component acting late in ironsulfur protein biogenesis. Structure 15: 12461257, 2007.
13. Gari K, León Ortiz AM, Borel V, Flynn H, Skehel JM and Boulton SJ: MMS19 links cytoplasmic ironsulfur cluster assembly to DNA metabolism. Science 337: 243245, 2012.
14. Stehling O, Mascarenhas J, Vashisht AA, Sheftel AD, Niggemeyer B, Rösser R, Pierik AJ, Wohlschlegel JA and Lill R: Human CIA2AFAM96A and CIA2BFAM96B integrate iron homeostasis and maturation of different subsets of cytosolic-nuclear ironsulfur proteins. Cell Metab 18: 187198, 2013.
15. Ritchie ME, Phipson B, Wu D, Hu Y, Law CW, Shi W and Smyth GK: limma powers differential expression analyses for RNAsequencing and microarray studies. Nucleic Acids Res 43: e47, 2015.
16. Robin X, Turck N, Hainard A, Tiberti N, Lisacek F, Sanchez J-C and Müller M: pROC: an open-source package for R and S+ to analyze and compare ROC curves. BMC Bioinformatics 12: 77, 2011.
17. Therneau T: A package for survival analysis in R. R package version 2, 2014.
18. Harrell FE: Regression modeling strategies. With Applications to Linear Models, Logistic Regression, and Survival Analysis. 1st edition. Springer, New York, NY, 2001.
19. Yu G, Wang LG, Han Y and He QY: clusterProfiler: An R package for comparing biological themes among gene clusters. Omics 16: 284287, 2012.
20. Stuart T, Butler A, Hoffman P, Hafemeister C, Papalexi E, Mauck WM III, Hao Y, Stoeckius M, Smibert P and Satija R: Comprehensive integration of singlecell data. Cell 177: 18881902. e21, 2019.
21. Mayakonda A, Lin DC, Assenov Y, Plass C and Koeffler HP: Maftools: Efficient and comprehensive analysis of somatic variants in cancer. Genome Res 28: 17471756, 2018.
22. Reinhold WC, Sunshine M, Liu H, Varma S, Kohn KW, Morris J, Doroshow J and Pommier Y: CellMiner: A webbased suite of genomic and pharmacologic tools to explore transcript and drug patterns in the NCI60 cell line set. Cancer Res 72: 34993511, 2012.
23. Villanueva RAM and Chen ZJ: ggplot2: Elegant Graphics for Data Analysis (2nd ed.). Measurement (Mahwah N J) 17: 160-167, 2019.
24. Livak KJ and Schmittgen TD: Analysis of relative gene expression data using realtime quantitative PCR and the 2(-Delta Delta C(T)) method. Methods 25: 402408, 2001.
25. Towbin H, Staehelin T and Gordon J: Electrophoretic transfer of proteins from polyacrylamide gels to nitrocellulose sheets: Procedure and some applications. Proc Natl Acad Sci USA 76: 43504354, 1979.
26. Brummelkamp TR, Bernards R and Agami R: A system for stable expression of short interfering RNAs in mammalian cells. Science 296: 550553, 2002.
27. Mosmann T: Rapid colorimetric assay for cellular growth and survival: Application to proliferation and cytotoxicity assays. J Immunol Methods 65: 5563, 1983.
28. Franken NA, Rodermond HM, Stap J, Haveman J and van Bree C: Clonogenic assay of cells in vitro. Nat Protoc 1: 23152319, 2006.
29. Justus CR, Leffler N, RuizEchevarria M and Yang LV: In vitro cell migration and invasion assays. J Vis Exp: 51046, 2014.
30. Pawley JB: Handbook of biological confocal microscopy. 3rd edition. Springer Science & Business Media, Berlin, 2006.
31. Shen W, Song Z, Zhong X, Huang M, Shen D, Gao P, Qian X, Wang M, He X, Wang T, *et al*: Sangerbox: A comprehensive, interaction-friendly clinical bioinformatics analysis platform. Imeta 1: e36, 2022.
32. Sipos K, Lange H, Fekete Z, Ullmann P, Lill R and Kispal G: Maturation of cytosolic iron-sulfur proteins requires glutathione. J Biol Chem 277: 26944-26949, 2002.

33. Morimoto RI: The heat shock response: Systems biology of proteotoxic stress in aging and disease. Cold Spring Harb Symp Quant Biol 76: 91-99, 2011.
34. Lianos GD, Alexiou GA, Mangano A, Mangano A, Rausei S, Boni L, Dionigi G and Roukos DH: The role of heat shock proteins in cancer. Cancer Lett 360: 114118, 2015.
35. Zhao Y, Bai Y, Shen M and Li Y: Therapeutic strategies for gastric cancer targeting immune cells: Future directions. Front Immunol 13: 992762, 2022.
36. Shitara K, Özgüroğlu M, Bang YJ, Di Bartolomeo M, Mandalà M, Ryu MH, Fornaro L, Olesiński T, Caglevic C, Chung HC, *et al*: Pembrolizumab versus paclitaxel for previously treated, advanced gastric or gastrooesophageal junction cancer (KEYNOTE061): A randomised, openlabel, controlled, phase 3 trial. Lancet 392: 123133, 2018.
37. Sexton RE, Al Hallak MN, Diab M and Azmi AS: Gastric cancer: A comprehensive review of current and future treatment strategies. Cancer Metastasis Rev 39: 11791203, 2020.
38. Bai R, Chen N, Li L, Du N, Bai L, Lv Z, Tian H and Cui J: Mechanisms of cancer resistance to immunotherapy. Front Oncol 10: 1290, 2020.
39. Petrillo A, Pompella L, Tirino G, Pappalardo A, Laterza MM, Caterino M, Orditura M, Ciardiello F, Lieto E, Galizia G, *et al*: Perioperative treatment in resectable gastric cancer: Current perspectives and future directions. Cancers (Basel) 11: 399, 2019.
40. Yuan X, Wang J, Huang Y, Shangguan D and Zhang P: Singlecell profiling to explore immunological heterogeneity of tumor microenvironment in breast cancer. Front Immunol 12: 643692, 2021.
41. Zhang Z, Shao S, Luo H, Sun W, Wang J and Yin H: The functions of cuproptosis in gastric cancer: Therapy, diagnosis, prognosis. Biomed Pharmacother 177: 117100, 2024.
42. Uhlen M, Zhang C, Lee S, Sjöstedt E, Fagerberg L, Bidkhori G, Benfeitas R, Arif M, Liu Z, Edfors F, *et al*: A pathology atlas of the human cancer transcriptome. Science 357: eaan2507, 2017.
43. Lill R, Dutkiewicz R, Elsässer HP, Hausmann A, Netz DJ, Pierik AJ, Stehling O, Urzica E and Mühlenhoff U: Mechanisms of iron-sulfur protein maturation in mitochondria, cytosol and nucleus of eukaryotes. Biochim Biophys Acta 1763: 652667, 2006.
44. Maio N, Orbach R, Zaharieva IT, Töpf A, Donkervoort S, Munot P, Mueller J, Willis T, Verma S, Peric S, *et al*: CIAO1 loss of function causes a neuromuscular disorder with compromise of nucleocytoplasmic Fe-S enzymes. J Clin Invest 134: e179559, 2024.
45. Johnstone RW, Wang J, Tommerup N, Vissing H, Roberts T and Shi Y: Ciao 1 is a novel WD40 protein that interacts with the tumor suppressor protein WT1. J Biol Chem 273: 1088010887, 1998.
46. Netz DJ, Stith CM, Stümpfig M, Köpf G, Vogel D, Genau HM, Stodola JL, Lill R, Burgers PM and Pierik AJ: Eukaryotic DNA polymerases require an ironsulfur cluster for the formation of active complexes. Nat Chem Biol 8: 125132, 2012.
47. Isaya G: Mitochondrial ironsulfur cluster dysfunction in neurodegenerative disease. Front Pharmacol 5: 29, 2014.
48. Shah NP, Tran C, Lee FY, Chen P, Norris D and Sawyers CL: Overriding imatinib resistance with a novel ABL kinase inhibitor. Science 305: 399-401, 2004.
49. Talpaz M, Shah NP, Kantarjian H, Donato N, Nicoll J, Paquette R, Cortes J, O'Brien S, Nicaise C, Bleickardt E, *et al*: Dasatinib in imatinib-resistant Philadelphia chromosome-positive leukemias. N Engl J Med 354: 2531-2541, 2006.
50. Dawson MA, Curry JE, Barber K, Beer PA, Graham B, Lyons JF, Richardson CJ, Scott MA, Smyth T, Squires MS, *et al*: AT9283, a potent inhibitor of the aurora kinases and Jak2, has therapeutic potential in myeloproliferative disorders. Br J Haematol 150: 46-57, 2010.
51. Deng J, Zhuang H, Shao S, Zeng X, Xue P, Bai T, Wang X, Shangguan S, Chen Y, Yan S and Huang W: Mitochondrial-targeted copper delivery for cuproptosis-based synergistic cancer therapy. Adv Healthc Mater 13: e2304522, 2024.